Iraqi Journal of Physics, 2022 *Vol.20, No.3, PP.1-12*

DOI: 10.30723/ijp.v20i3.1001 *P-ISSN: 2070-4003*
E-ISSN: 2664-5548

Producing Hydrogen Energy Using Cr_2O_3-TNFs Nanocomposite with Animal (Chitosan) Extract via Ultrasonic and Hydrothermal Techniques

Ghasaq Z. Alwan[1a*], Wisam J. Aziz[1b] and Raad S. Sabry[1c]
[1]*Department of Physics, College of Science, University of Mustansiriyah, Baghdad, Iraq*
[b]E-mail: wisamjafer14@gmail.com, [c]E-mail: raadsaadon74@gmail.com
[a*]Corresponding Author: Gasaq.zuher@gmail.com

Abstract

In this study, an efficient photocatalyst for dissociation of water was prepared and studied. The chromium oxide (Cr_2O_3) with Titanium dioxide (TiO_2) nanofibers (Cr_2O_3-TNFs) nanocomposite with (chitosan extract) were synthesized using ecologically friendly methods such as ultrasonic and hydrothermal techniques; such TiO_2 exhibits nanofibers (TNFs) shape structure. Doping TiO_2 with chromium (Cr) enhances its ability to absorb ultraviolet light while also speeding up the recombination of photogenerated electrons and holes. The prepared TNFs and Cr_2O_3-TNFs were characterized by X-ray diffraction (XRD), field emission scanning electron microscopy (FE-SEM), energy dispersive X-ray spectroscopy (EDX), and UV-Visible absorbance. The XRD of TNFs showed a tetragonal phase with 6.9 nm of average crystallite size, whereas Cr_2O_3-TNFs crystallite size was 12.3 nm. FE-SEM images showed that the average particle size of TNFs was in the range of (9-35) nm and UV-Vis absorbance of TNFs showed their energy gap to be 3.9eV while the energy gaps of Cr_2O_3-TNFs were smaller equal to 2.4 eV. The highest hydrogen production rate for the Cr_2O_3-TNFs nanocomposite was 4.1ml after 80min of UV exposure. Cr_2O_3-TNFs have high photocatalytic effectiveness due to their wide ultraviolet light photoresponse range and excellent separation of photogenerated electrons and holes.

Article Info.

Keywords:
Cr_2O3-TNFs nanocomposite, chitosan extract, hydrothermal technique, photocatalyst, hydrogen production.

Article history:
Received: Apr. 30, 2022
Accepted: Jun. 9, 2022
Published: Sep. 01,2022

1. Introduction

Fossil fuel usage has recently become a source of concern, both in terms of its existence and its long-term viability, as well as its impact on the environment. Alternative energy sources that are renewable and eco-friendly are required for future community growth. The sun is the world's largest and most affordable (free) energy source. It has the potential to be a renewable energy source. Various technologies for solar energy conversion and usage have been tested. Solar energy has long been regarded as the most efficient and environmentally friendly method of producing hydrogen. Fuel cells can use the hydrogen, produced from the splitting of water using solar energy to generate energy. The efficiency of solar water separation device become the primary fuel for a renewable energy economy, must be enhanced if solar energy will play a significant role in the production of clean fuels (hydrogen). In order for hydrogen to become the primary fuel for a renewable energy economy in the future, high-capacity hydrogen storage technology and high-performance fuel cells, must be created [1]. In this case, photocatalytic water splitting into O_2 and H_2 is a viable option [2]. Because of its zero-emissions and long-term viability, hydrogen is highly regarded as a fuel. Titanium dioxide (TiO_2) has long been the most extensively used photocatalyst for hydrogen generation because of its stability, corrosion resistance, purity (no contaminates), natural availability, and low cost [3, 4]. The photocatalytic activity of TiO_2 has been reported to be improved by heteroatom doping [5], alternation of the surface [6, 7], co-catalysts for loading [8, 9], and

heterojunctions creation [10, 11]. It has substantial band-gap energy (anatase 3.2 eV and rutile 3.0 eV). Under UV light irradiation, TiO_2 has been widely employed as a photocatalyst for photocatalytic water splitting to create hydrogen [12]. UV light stimulates electrons from the valence band into the conduction band, resulting in the formation of electron-holes pairs [13]. However, it has a high photogenerated electron-hole pair recombination rate and a limited visible light absorption capacity. Only hydrogen derived from water may be considered an ecologically beneficial energy carrier among these basic sources. When hydrogen is created from water and then burnt, it produces no CO_2 [14, 15]. TiO_2 has been modified with transition-metal cations to increase its absorption capacity for light hence its photocatalytic capabilities [16, 17]. Several studies have suggested adding chromium oxide to titanium oxide to improve the effectiveness of photocatalysis [18]. Cr_2O_3 has generally been considered a good photocatalytic material for ultraviolet light because of its tight bandgap, and thus, it has been considered as a TiO_2 dopant [17, 19]. Cr^{3+} was mixed with TiO_2 powder to increase its photocatalytic capabilities [20]. In this study, animal extract (chitosan) was used to synthesize Cr_2O_3-TiO_2 using impregnation technique. It is possible to detect some of the most important constituents in the animal extract (chitosan), includes basic totals found in the rutin (Rutin is a quercetin rutinoside with glucose and rhamnose sugar groups replacing the hydroxy group at position C-3) vitamin C, and cellulose are also included in chitosan, which are significant components of the chitosan extract [21]. To reduce $Cr(NO_3)_3$ hydroxide, chitosan extract partially reduces $Cr(NO_3)_3$ hydroxide to generate Cr_2O_3-TiO_2 nanocomposite. The objectives of this work are to synthesise Cr_2O_3-TNFs nanocomposite and improve photogenerated electron–hole pair efficiency and photocatalytic activity by improving optical responsiveness in ultraviolet range.

2. Experimental work

2.1. Synthesis of TiO_2 nanofibers

Commercial TiO_2 nanoparticles (from Sky spring Nanomaterial, Inc.) were used as the starting point for the fabrication of TiO_2 nanofibers. The hydrothermal technique was used to synthesize TiO_2 utilizing both hydrochloric acid (HCl) and sodium hydroxide (NaOH) [10]. First, 3 g of TiO_2 was dispersed with ultrasonic-assistance in 100 ml of NaOH (10 M) for 30 minutes, with stirring for 4 hrs. After that, the suspension was placed in a Teflon-lined autoclave container and incubated at 180 °C. The reaction duration was 8 hrs for hydrothermal treatment. The final product was treated with 1.5 ml of HCl overnight and then washed with deionized water until the pH reached 7. After that, the material was filtered and dried at 60°C.

2.2. Preparation of the animal extract (chitosan)

0.5 g of chitosan was dissolved in acetic acid in the water of 1:50 ratio and mixed with the ultrasonic tool for 2 hrs, then filtered using micro porous membrane (pore sizeo0.22μm). The solution was centrifuged at 4000 rpm for 5 minutes to remove any residual salts and impurities.

2.3. Preparation of the Cr_2O_3-TiO_2 nanocomposites using animal extract (chitosan)

Cr_2O_3-TNFs nanocomposite was synthesized using 0.0329 g of $Cr(NO_3)_3.9H_2O$ with 2 ml anhydrous ethanol solution and 1ml of chitosan extract treated to produce a clear dark blue solution that was then impregnated with 2.5 g of (TNFs). The impregnate was volatilized at 70°C until being annealed for 2 hrs at 300°C.

2.4. Characterization of Cr_2O_3-TiO_2 nanocomposites

Cr_2O_3-TiO_2 nanocomposites were characterized with UV-Visible spectrometer type (DU- 8800D- China) within the wavelength range (190-1100) nm and with X-ray diffractometer (SHIMADZU, XRD - 6000, JAPAN) using CuKα radiation (λ=1.5406 Å). While the morphological properties of Cr_2O_3-TiO_2 nanocomposites were studied with a Field Emission Scanning Electron Microscope (FESEM INSPECT F-50, Company FEI, Dutch) and with energy dispersive (X-Ray) spectroscopy (EDX).

2.5. The assessment of photocatalytic hydrogen generation

As shown in Fig.1, the laboratory cell that was used to separate hydrogen from the water was made locally from quartz glass (6 cm x 28 cm) and consisted of a hydrogen gas cylinder. The cylinder is equipped with holes for the exit of gas; water decomposition was carried out using an analytical system, such that the quantity of photocatalyst measured was 2 g from the Cr_2O_3-TiO_2 placed in a quartz flask containing 500 ml of water and 0.028 M KOH of a sacrificial reagent aqueous solution (Cr_2O_3-TiO_2), which was exposed to ultraviolet light irradiation (λ<400 nm).

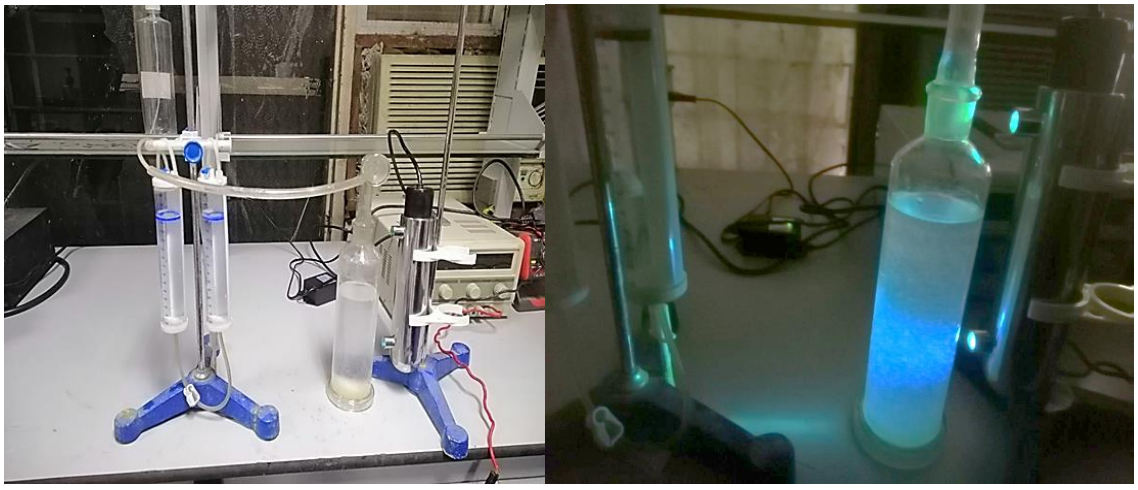

Figure 1: The local fuel cell used to generate hydrogen from water.

3. Results and discussion

3.1. XRD analysis of TNFs and Cr_2O_3 -TNFs nanocomposite

The XRD pattern of TNFs revealed the planes (101), (103), (004), (112), (200), (105), (211), (204), and (116) with 2θ values of (25.2°), (36.9°), (37.8°), (38.0°), (48.4°), (53.7°), (55.2°), (62.6°), and (68.5°), respectively, as shown in Fig.2 .The diffraction peaks revealed a tetragonal anatase phase, according to (JCPDS No..84-1285). The strongest diffraction peak at (25.2°) indicated (101) plane of anatase TiO_2 of two patterns, anatase structure by the peaks other than (53.7°), and (55.2°), and rutile structure indicated by the peaks 53.7° and 55.2°. This suggests that the anatase is the dominant crystal phase in TiO_2 nanoparticles, with the presence of some rutile phases in small amounts in the final product. These findings align with the previous research project by Ahmad et al. [20]. The TNFs, average crystallite size, as found by Scherrer's formula [22], was equal to 6.3 nm.

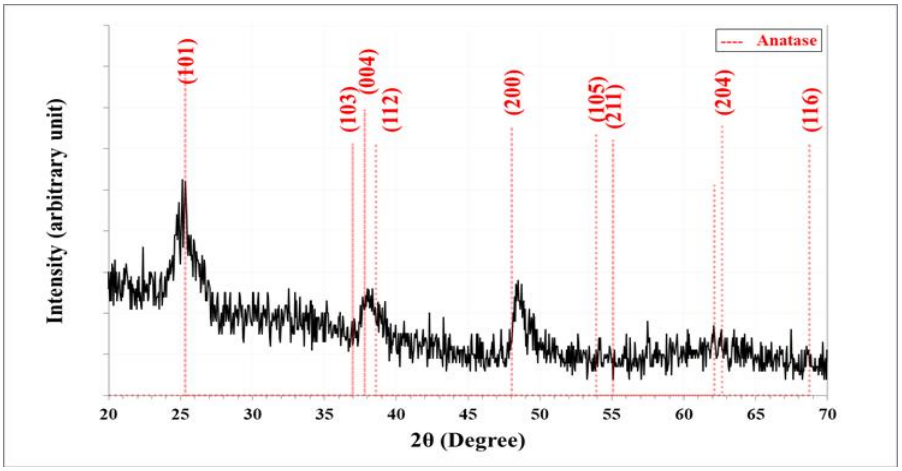

Figure 2: XRD patterns of TNFs

Fig.3 illustrates the XRD pattern of Cr_2O_3-TNFs nanocomposite heterostructures at different Cr_2O_3 percentages. The diffraction planes (101), (103), (004), (112), (200), (105), (211), (204), and (116) (JCPDS Card NO. 84-1285), corresponding to 2θ =(24.9°), (36.6°), (37.75°), (38.1°), (48.2°), (53.9°), (55.4°), (62.7°) and (68.5°), respectively are seen in the crystallized anatase phase of Cr_2O_3-TNFs. Because of the small proportions of Cr_2O_3 nanoparticles relative to the TiO_2, the XRD patterns showed peaks of Cr_2O_3 at 2θ = (33.3°), and (44.6°) (JCPDS No. 1308-38-9). According to these findings, the successful modification of titanium dioxide by the addition of Cr_2O_3 has created flaws in the anatase crystal to form Ti-O-Cr bonds which allowed it to interact with both Cr^{3+} ions and TiO_2 [23]. As a result, it was concluded that the presence of Cr_2O_3 blocked the pore wall of TiO_2. The crystal size of Cr_2O_3-TNF was 12.3 nm. These results showed that the crystal size of TiO_2 increased when loaded with Cr_2O_3.

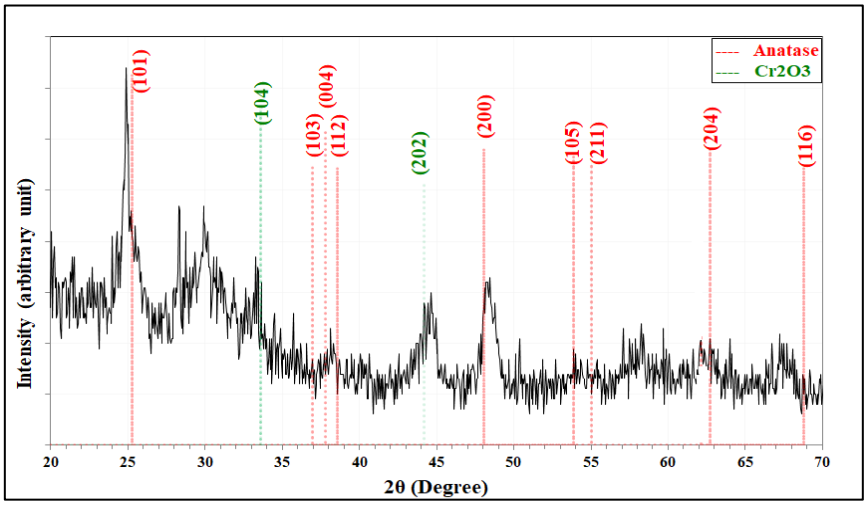

Figure 3: XRD patterns of Cr_2O_3-TNFs nanocomposites.

3.2. FE-SEM images of TNFs and Cr_2O_3-TNFs nanocomposites with chitosanextract

The morphology of TNFs, as seen from the FESEM images Fig.(4-A) appears as fibers with few rods and a few aggregations. The average particle size appeared to be between 9 and 35 nm (measured using Image J software). Fig.(4-B) shows Cr_2O_3 with TNFs (rod shapes) nanocomposites. The bonding of chromium and titanium oxide

particles by weak forces leads to the agglomeration of the nanoparticles and the formation of a large surface area [23].

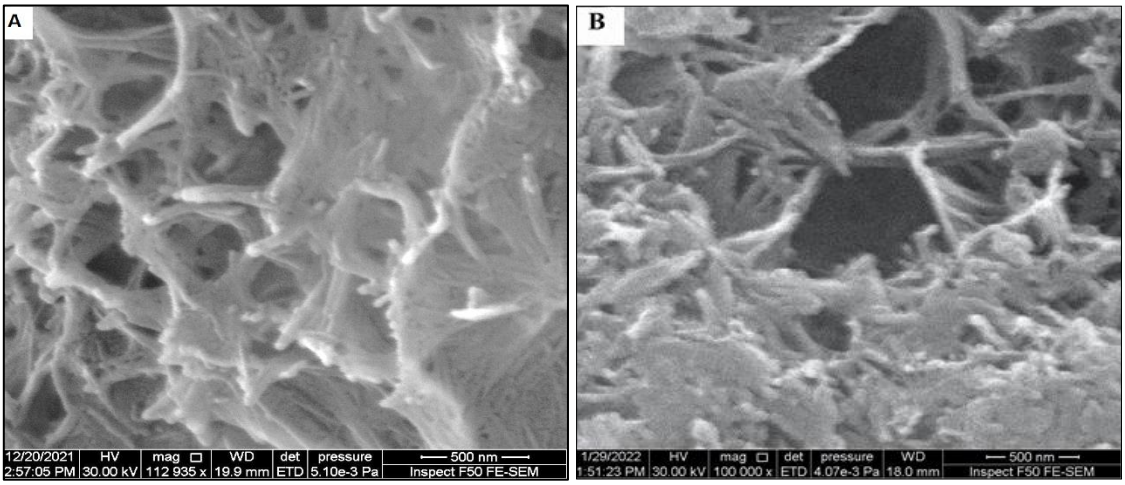

Figure 4: FE-SEM images of (A) TNFs (B) Cr_2O_3 - TNFs nanocomposite.

3.3. EDX of of TNFs and Cr_2O_3-TNFs nanocomposites

EDX analyses of TNPs and Cr_2O_3 with TNFs nanocomposite are shown in Figs. 5 and Tables 1. It reveals the characteristic emission peaks for Ti ,O_2 and Cr, in addition to peaks related to C and to some trace elements observed in both samples as a residual from the extracted material, which may be associated with the presence of phytomolecules (polyphenols, alkaloids, and flavonoids) of chitosan extracts adsorbed on TNFs surface.

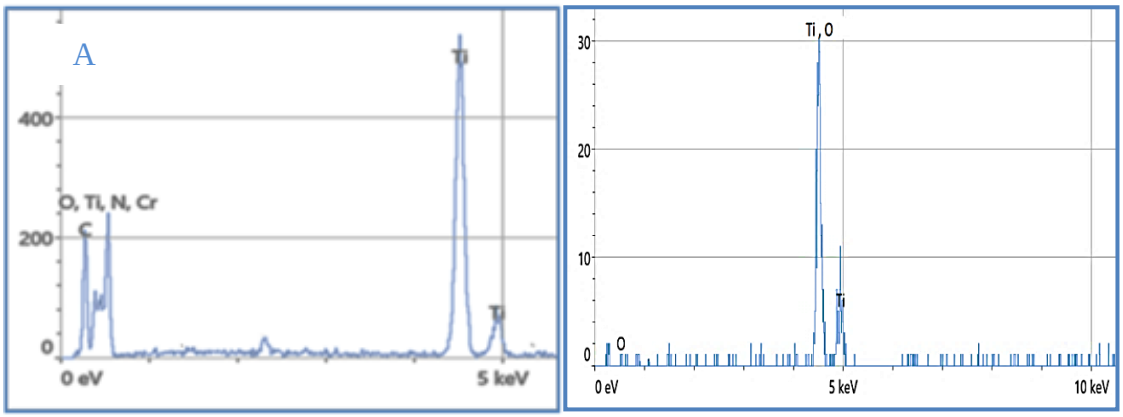

Figure 5: The elements, atomic and weight ratios of (A) TNFs and (B) Cr_2O_3-TNFs

Table 1: The elements, atomic and weight ratios of TNFs and Cr_2O_3 with TNFs.

Element	TNFs		Cr_2O_3-TNFs	
	Atomic %	Weight %	Atomic %	Weight %
O	51.0	75.7	56.5	49.4
Ti	49.0	24.3	11.2	33.3
Cr	–	–	0.1	0.5
N	–	–	5	2.8
C	–	–	27.2	14

Fig.6 depicts the UV-Visible absorption spectra of samples where the TNFs samples exhibit an absorption edge at 310 nm. The energy gap was calculated using the Tauc formula, which was equal to 3.9 eV for TNFs, as shown in Fig.7. Fig.8 shows that loading TNFs with Cr^{3+} improved their absorption in the ultraviolet region. The absorption bands for Cr_2O_3-TNFs were around 409 nm; the energy gap of Cr_2O_3- TNFs was 2.4 eV, as shown in Fig.9. The absorption edge of the Cr_2O_3-TNFs nanocomposite with chitosan extract shifted to higher wavelength in the visible region as compared to that of the pure TNFs. It may be concluded that proper Cr doping resulted in the narrowing of the anatase TiO_2 band gap. The introduction of dopant levels is the cause of the narrower bandgap. This would also cause an electron to be excited from the valence band to the dopant levels. Cr doping may also act as an electron-capture trap, preventing recombination of electron-hole pairs. Cr doping, on the other hand, produces deep dopant levels, and recombination sites that can speed up the recombination of electron-hole pairs. These results agree with those of Zhu et al. [24].

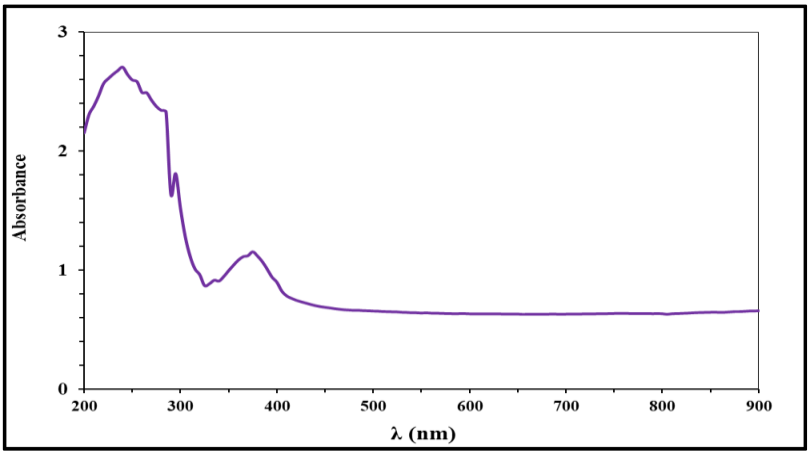

Figure 6: Ultraviolet-Visible absorption spectra of the TNFs.

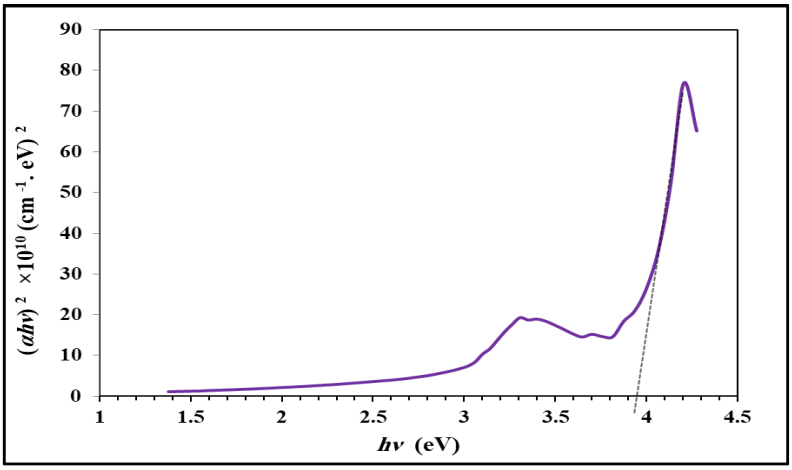

Figure 7: The energy gap of (TNFs).

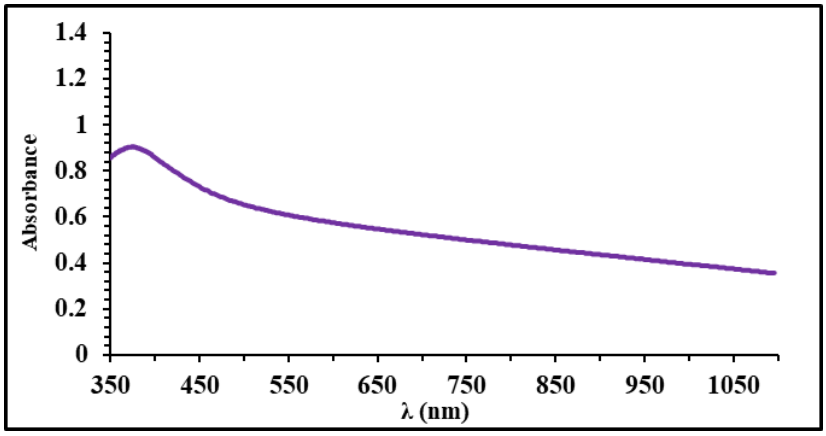

Figure 8: Ultraviolet-Visible absorption spectra of Cr_2O_3 with TNFs.

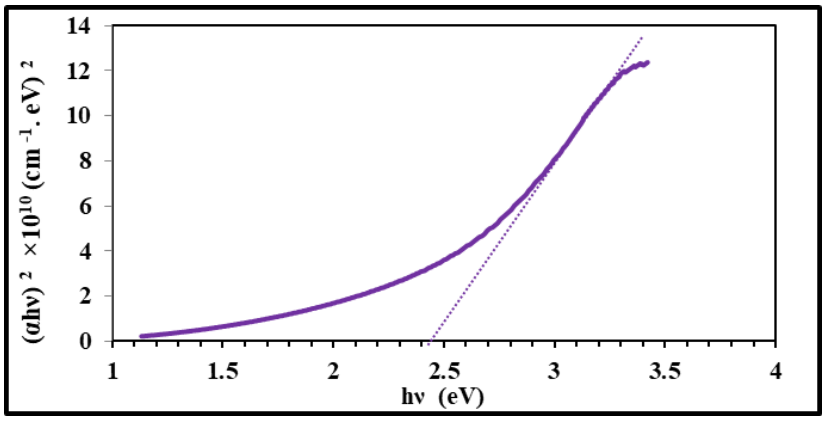

Figure 9: The energy gap of Cr_2O_3 with TNFs.

3.4. Activity of hydrogen production

The photocatalytic decomposition of water under ultraviolet irradiation for different times (10-80) min generated hydrogen from Cr_2O_3-TNFs nanocomposite as shown in Fig.10. The activity of the Cr_2O_3-TNFs photocatalyst increased with increasing exposure time (Table 2). The Cr_2O_3-TNFs photocatalyst has the highest H_2 production (4.1 ml) was at (80 min) while the low H_2 production (0.4ml) at (20min). It is noted that hydrogen is not produced after 10 min of reaction time. The effectiveness of the components (such as salts and oxides of transition metals) for many catalysts is spontaneously dispersed on the surface of the carriers. The production of hydrogen gas is twice the production of oxygen gas during the photocatalytic process due to the effectiveness of the reaction of Cr_2O_3-TNFs nanocomposite.

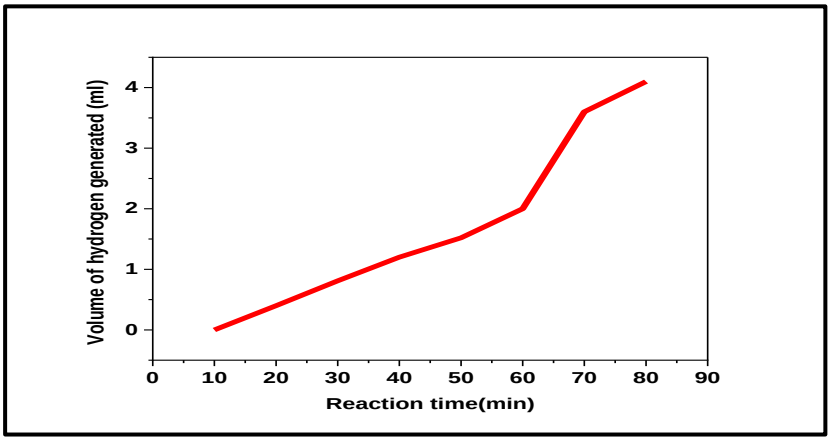

Figure 10: Time courses of hydrogen evolution over Cr_2O_3-TNFs photocatalysts using chitosan extract under irradiation.

Table 2: Summary volume of hydrogen generated (ml) and reaction time of (Cr_2O_3 –TNFs) photocatalysts using chitosan extract detected via laboratory cell and it is measured by liquid displacement

Cr_2O_3-TNFs Volume of hydrogen generated (ml)	**Reaction time(min)**
0	0
0.4	20
0.81	30
1.2	40
1.52	50
2	60
3.6	70
4.1	80

3.5. The mechanism of photocatalytic hydrogen generation using Cr_2O_3-TNFs nanocomposite.

Fig. 11 illustrates the mechanism for the photocatalytic decomposition of water to produce hydrogen using Cr_2O_3-TNFs nanocomposite. The photogenerated electron (e-) moving from Cr^{3+} ions donor level to the conduction band of TNFs, absorbs energy from an ultraviolet photon as described in Eq.(1). Photogenerated electrons move from TNFs' conduction band (CB) to their surface, where they reduce H_2O molecules to form H_2 and OH^- ions, as in Eq.(2). Meanwhile, photogenerated holes transferred from TNFs' valence band (VB) to the donor level Cr^{3+} which oxidize by H_2O molecules, yielding O_2 and H^+ ions, as illustrated in Eq. (3). It gives more stability to the reaction and the reducing agent for Cr^{3+} ions. The addition of an optimal quantity of Cr^{3+} ions species to the surface of TNFs may lower the recombination rate of photogenerated electron–hole pairs by increasing their separation efficiency, and boosting photocatalytic activity [25].

$$\mathbf{Cr^{3+} + hv \rightarrow e^- + h^+} \qquad (1)$$

$$\mathbf{H_2O + e\text{-} \rightarrow \frac{1}{2}H^2 + OH^-} \qquad (2)$$

$$H_2O + h^+ \rightarrow \frac{1}{2}O_2 + 2H^+ \qquad (3)$$

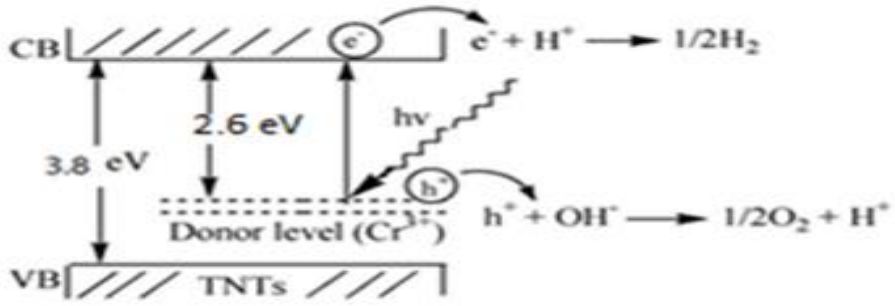

Figure 11: Photocatalytic hydrogen generation mechanism.

4. Conclusions

Hydrothermal and ultrasonic processes were used to create a variety of Cr_2O_3-TiO_2 nanocomposites. An XRD and FESEM analysis of prepared nanocomposites showed that they contained a mixture of Cr_2O_3-TiO_2 (nanofibers). The average diameter of nanofibers was (9-35) nm. The absorption edges of TNFs were extended to visible light region by doping with Cr_2O_3. The energy gap was equal to 3.9 eV, which is larger than the energy gap of Cr_2O_3-TNFs 2.4 eV because of the appropriate Cr doping that resulted in the narrowing of the band gap of the anatase TNFs. Briefly, it has succeeded in synthesizing environmentally friendly biomolecules via ultrasonic and hydrothermal methods. If the effect of the morphology of the compound Cr_2O_3-TiO_2 was in the form of nanofibers, it was discovered to have an effect on the performance of the current work, where the compound showed a distinguished performance in hydrogen production through photocatalysts (4.1ml) at 80min. It can be concluded from this work that nanofibers with a large surface area have the ability to make hydrogen; this is largely dependent on the amount of Cr^{3+} that can be added to the TNFs.

Acknowledgements

The authors would like to thanks Al-Mustansiriayah University/College of Science /Physics Department / Baghdad-Iraq.

Conflict of interest

Authors declare that they have no conflict of interest.

References

1. Mao S.S. and Chen X., *Selected nanotechnologies for renewable energy applications.* International journal of energy research, 2007. **31**(6-7): pp. 619-636.
2. Feil A.F., Migowski P., Scheffer F.R., Pierozan M.D., Corsetti R.R., Rodrigues M., Pezzi R.P., Machado G., Amaral L., and Teixeira S.R., *Growth of TiO_2 nanotube arrays with simultaneous Au nanoparticles impregnation: photocatalysts for hydrogen production.* Journal of the Brazilian Chemical Society, 2010. **21**(7): pp. 1359-1365.

3. Acar C., Dincer I., and Naterer G.F., *Review of photocatalytic water-splitting methods for sustainable hydrogen production.* International Journal of Energy Research, 2016. **40**(11): pp. 1449-1473.
4. Cushing S.K., Li J., Meng F., Senty T.R., Suri S., Zhi M., Li M., Bristow A., and Wu N., *Photocatalytic activity enhanced by plasmonic resonant energy transfer from metal to semiconductor.* Journal of the American Chemical Society, 2012. **134**(36): pp. 15033-15041.
5. Chen Y., Li A., Li Q., Hou X., Wang L.-N., Huang Z.-H., and technology, *Facile fabrication of three-dimensional interconnected nanoporous N-TiO_2 for efficient photoelectrochemical water splitting.* Journal of materials science, 2018. **34**(6): pp. 955-960.
6. Wang H., Hu X., Ma Y., Zhu D., Li T., and Wang J., *Nitrate-group-grafting-induced assembly of rutile TiO_2 nanobundles for enhanced photocatalytic hydrogen evolution.* Chinese Journal of Catalysis, 2020. **41**(1): pp. 95-102.
7. Wang P., Xu S., Chen F., and Yu H., *Ni nanoparticles as electron-transfer mediators and NiSx as interfacial active sites for coordinative enhancement of H2-evolution performance of TiO_2.* Chinese Journal of Catalysis, 2019. **40**(3): pp. 343-351.
8. Shen J., Wang R., Liu Q., Yang X., Tang H., and Yang J., *Accelerating photocatalytic hydrogen evolution and pollutant degradation by coupling organic co-catalysts with TiO_2.* Chinese Journal of Catalysis, 2019. **40**(3): pp. 380-389.
9. Meng A., Zhang L., Cheng B., and Yu J., *Dual cocatalysts in TiO_2 photocatalysis.* Advanced Materials, 2019. **31**(30): pp. 1-31.
10. Li H., Zhou Y., Tu W., Ye J., and Zou Z., *State-of-the-art progress in diverse heterostructured photocatalysts toward promoting photocatalytic performance.* Advanced Functional Materials, 2015. **25**(7): pp. 998-1013.
11. Zhang W., Zhang H., Xu J., Zhuang H ,.and Long J., *3D flower-like heterostructured TiO_2@$Ni(OH)_2$ microspheres for solar photocatalytic hydrogen production.* Chinese Journal of Catalysis, 2019. **40**(3): pp. 320-325.
12. Malato S., Fernández-Ibáñez P., Maldonado M.I., Blanco J., and Gernjak W ,. *Decontamination and disinfection of water by solar photocatalysis: recent overview and trends.* Catalysis today, 2009. **147**(1): pp. 1-59.
13. Camelia C., Daniela J., Eliza G.S., Irina-Draga C., Florin Z.E., Carmen C., Cristina T., Anca V., and Eugen C., *Colonic carcinoma microenvironment: immunohistochemical frequency and distribution of CD3, CD8, FOXP3 infiltrating T lymphocytes.* Revista Română de Medicină de Laborator, 2010. **18**(4/4): pp. 7-16.
14. Mazloomi K. and Gomes C., *Hydrogen as an energy carrier* :*Prospects and challenges.* Renewable and Sustainable Energy Reviews, 2012. **16**(5): pp. 3024-3033.
15. Ipsakis D., Voutetakis S., Seferlis P., Stergiopoulos F., and Elmasides C., *Power management strategies for a stand-alone power system using renewable energy sources and hydrogen storage.* International journal of hydrogen energy, 2009. **34**(16): pp. 7081-7095.
16. Wang B., Wang Z., Cui Y., Yang Y., Wang Z., Chen B., and Qian G., *Cr_2O_3@TiO_2 yolk/shell octahedrons derived from a metal–organic framework for high-performance lithium-ion batteries.* Microporous and Mesoporous Materials, 2015. **203**: pp. 86-90.

17. Huang H., Wang Z., Luo B., Chen P., Lin T., Xiao M., Wang S., Dai B., Wang W., and Kou J., *Design of twin junction with solid solution interface for efficient photocatalytic H_2 production.* Nano Energy, 2020. **69**: pp. 1-9.
18. Tsegay M., Gebretinsae H., and Nuru Z., *Structural and optical properties of green synthesized Cr_2O_3 nanoparticles.* Materials Today: Proceedings, 2021. **36**: pp. 587-590.
19. Mao G., Xu M., Yao S., Zhou B., and Liu Q., *Direct growth of Cr-doped TiO_2 nanosheet arrays on stainless steel substrates with visible-light photoelectrochemical properties.* New Journal of Chemistry, 2018. **42**(2): pp. 1309-1315.
20. Ahmad M.M., Mushtaq S., Al Qahtani H.S., Sedky A., and Alam M.W., *Investigation of TiO_2 Nanoparticles Synthesized by Sol-Gel Method for Effectual Photodegradation, Oxidation and Reduction Reaction.* Crystals, 2021. **11**(12): pp. 1-16.
21. Bharathi D., Ranjithkumar R., Vasantharaj S., Chandarshekar B., and Bhuvaneshwari V., *Synthesis and characterization of chitosan/iron oxide nanocomposite for biomedical applications.* International journal of biological macromolecules, 2019. **132**: pp. 880-887.
22. Tsegay M., Gebretinsae H., and Nuru Z., *Structural and optical properties of green synthesized Cr_2O_3 nanoparticles.* Materials Today: Proceedings, 2021. **36**: pp. 587-590.
23. Alzahrani K.A., Mohamed R.M., and Ismail A.A., *Enhanced visible light response of heterostructured Cr_2O_3 incorporated two-dimensional mesoporous TiO2 framework for H2 evolution.* Ceramics International, 2021. **47**(15): pp. 21293-21302.
24. Zhu H., Tao J., and Dong X., *Preparation and photoelectrochemical activity of Cr-doped TiO_2 nanorods with nanocavities.* The Journal of Physical Chemistry C, 2010. **114**(7): pp. 2873-2879.
25. Engge Y., Maulana F., and Nurhuda M. *Dissociation of water into hydrogen and oxygen through a combination of electrolysis and photocatalyst*. in *IOP Conference Series: Earth and Environmental Science*. 2021. IOP Publishing.

انتاج طاقة الهيدروجين باستخدام المركب النانوي Cr_2O_3 – TNFs مع مستخلص الشيتوزان الحيواني عبر تقنيتي الهيدروثيرمل والموجات الفوق الصوتية

غسق زهير علوان[1]، وسام جعفر عزيز[1]، رعد سعدون صبري[1]
قسم الفيزياء, كلية العلوم, الجامعة المستنصرية

الخلاصة

في هذه الدراسة تمت مناقشة كفاءة المحفزات الضوئية لفصل جزيئات الماء. تم تخليق المركب النانوي (Cr_2O_3 مع TNFs مع مستخلص الشيتوزان) باستخدام تقنيات صديقة للبيئة مثل هايدروثيرمل والموجات الفوق الصوتية, حيث ظهرت بنية ثنائي اوكسيد التيتانيوم TiO_2 على شكل الياف نانوية. ان مادة المركب النانوي تعزى الى قدرتها على امتصاص الاشعة الفوق البنفسجية وايضا تسريع اعادة الالتحام زوج الكترون - فجوة المتولد. تم وصف TNFs والمركب النانوي (Cr_2O_3-TNFs) بواسطة X-ray و UV و EDX و FE-SEM ووجد ان TNFs ذات طورروباعي الاضلاع ويمتلك حجم بلوري 6.9 nm بينما الحجم البلوري للمركب النانوي 12.3 nm واظهرت صور FE-SEM ان حجم الجسيمات النانوية nm (9-35). ولوحظ من خلال الامتصاص المرئي – الاشعة الفوق بنفسجية ان فجوة الطاقة TNFs مقدارها eV (3.9) بينما فجوة الطاقة للمركب النانوي اقل من ذلك ومقدارها eV (4.2). وجد ان اداء المحفزات الضوئية للمركب النانوي لانتاج الهيدروجين كان متفوقآ, حيث اعطى اعلى نسبة لانتاج الهيدروجين 4.1 ml في 80 min عند تعرضه للاشعة فوق البنفسجية,

اضافة الى ذلك, اظهر المركب النانوي نسبة انتاج عالية تحت التشعيع الفوق البنفسجي ذات الطول الموجي الاقل من 400 nm. ان المركب النانوي Cr_2O_3-TNFs يمتلك فعالية عالية للتحفيز الضوئي الناتج من قدرة الامتصاص العالية للضوء الفوق البنفسجي والفصل الممتاز لزوج الالكترون – فجوة.